MRS Advances (2023) 8:996–1003
https://doi.org/10.1557/s43580-023-00667-2

ORIGINAL PAPER

Morphological and mechanical characterization of a novel porous silicon membrane used in a lung-on-a-chip system

Sahra Genc[1] · Sally Thompson[1] · Owen Hill[1] · Leif Gislason[1] · Dakota Rodriguez[1] · Farjana Showme[1] · Alex Motler[1] · Sarah M. Schreiner[2,3] · Adrian Gestos[4] · Virginia L. Ferguson[4] · Jeff Jessing[1]

Received: 28 May 2023 / Accepted: 11 October 2023 / Published online: 23 October 2023

Abstract

In the last decade, organ-on-a-chip technology has been researched as an alternative to animal and cell culture models (Buhidma et al. in NPJ Parkinson's Dis, 2020; Pearce et al. in Eur Cells Mater 13:1–10, 2007; Huh et al. in Nat Protoc 8:2135–2157, 2013). While extensive research has focused on the biological functions of these chips, there has been limited exploration of functional materials that can accurately replicate the biological environment. Our group concentrated on a lung-on-a-chip featuring a newly fabricated porous silicon bio-membrane. This bio-membrane mimics the interstitial space found between epithelial and endothelial cells in vivo, with a thickness of approximately 1 µm (Ingber in Cell 164:1105–1109, 2016). This study aims to establish a fabrication method for producing a thin, uniform porous silicon membrane with a predictable *reduced modulus*. We conducted mechanical and morphological characterization using scanning electron microscopy and nanoindentation. A small, parametric study was conducted to determine the reduced modulus of the porous silicon and how it may relate to the morphological features of the membrane. We compare our results to other works.

Introduction

In the field of biomedical research, significant progress has been made in recent years to enhance our understanding of disease pathology and treatment strategies [1–3]. However, many of these advancements have relied on animal models and traditional cell culture techniques, which often fail to mimic human anatomy and physiology [4, 5]. As a result, there is a critical need for advanced model systems that are better at predicting the efficacy of potential treatment options. To close this knowledge gap, researchers have turned their attention to organ-on-a-chip technology, which offers a solution for the development of personalized medicine. By replicating the complex microenvironment and cellular interactions found in human organs, these devices provide a more accurate platform for studying diseases drug responses and the development of targeted therapies [5].

This paper focuses specifically on the fabrication and characterization of porous silicon (PSi) to create bio membranes for application in Lung-on-a-Chip models. The objective of this research is to establish a fabrication method for creating thin and uniform PSi membranes with predictable mechanical properties which closely mimics the interstitial space between epithelial and endothelial cells in the lungs. By optimizing the fabrication process, we aim to contribute to the development of Lung-on-a-Chip models that can advance personalized medicine and improve our understanding of lung-related diseases.

Materials and methods

Electrochemical anodization

In our study, we used (100) orientation p-type silicon wafers with a resistivity of 0.08–0.12 Ω cm and thickness of 279 ± 25 µm. The fabrication process began with the cleaning of the silicon wafers using acetone, isopropanol, and methanol

✉ Jeff Jessing
jrjessing@fortlewis.edu

1 Department of Physics and Engineering, Fort Lewis College, Durango, CO, USA

2 STROBE NSF Science and Technology Center, Boulder, USA

3 JILA, University of Colorado Boulder, Boulder, CO, USA

4 Department of Mechanical Engineering, University of Colorado Boulder, Boulder, CO, USA

followed by the application of a nitrogen gun for drying purposes.

Before the electrochemical anodization, a thinning process involving the use of potassium hydroxide (KOH) is typically performed [6]. However, for this specific study, we did not utilize the same procedure which is discussed in detail in previous work [6]. Detailed information regarding the thinning process is provided in the supplemental materials section, along with a schematic illustration for clarity.

We used a single-sided cell setup for anodization, as shown in Fig. 1a**.** The single-sided cell was made with polytetrafluoroethylene (PTFE) materials that held a clean wafer placed on top of a platinum sheet. The platinum sheet is pre-treated with a drop of hydrofluoric acid (HF) which aids in the removal of the wafer backside native oxide hence lowering the anodization electrical resistance. The top PTFE part, ultimately holding the HF solution, is then positioned onto the wafer, clamping the top and bottom parts together.

To initiate the anodization process, a mixture consisting of 1.5 parts 48% HF to 1 part ethanol is employed. To ensure consistency with our recent studies and obtain comparable results, a current density of 90 mA/cm^2 was applied over a cell diameter of 10 mm corresponding to an anodization area of approximately 0.785 cm^2 [6]. This specific configuration allowed us to achieve an etch rate of approximately 4.7 µm/min. For this study, we chose to anodize only partially through the wafers (i.e., not through-etched to the backside), as will be justified in the Results and Discussion section. Samples labeled as Ps_1 – Ps_5 were anodized for different times ranging from 672 to 13 s while all other parameters remained the same. These times were selected to target specific thicknesses of porous silicon. Further, in our previous studies [6], a current density of 90 mA/cm^2 was established as the optimal condition for creating micropores for epithelial and endothelial cell plating. To ensure consistency and enable comparisons with our previous research, we maintained this established current density for the present study.

Characterization of membrane and morphology

A JEOL 7100F scanning electron microscope (SEM) was used to image the anodized wafers to allow assessment of thickness, pore size, pore depth, and surface porosity. The surface porosity is defined as the ratio of the two-dimensional pore (*i.e.*, void) area to total area on the surface of the sample (refer to Fig. 1b). Larger values represent a higher degree of porosity in the sample. To determine the achieved pore depths after anodization, we performed SEM measurements within a 5 mm field, covering the center, left, and right regions of each sample. A total of 5 measurements were taken from each sample to ensure reliable statistical data.

To estimate the surface porosity of each sample, two-dimensional image analysis was performed on images taken with the SEM. For this analysis, five images were taken of each sample, with each image showing a different region within the 5 mm field. An example SEM image from our study is shown in Fig. 2a. The images were first modified in Adobe Photoshop using the *median noise reduction tool* to reduce visual noise (see Fig. 2b). Then, using ImageJ software [7], the brightness of each image was shifted to match the peak histogram values of every image to one another. Each image had the same brightness range with pixels ranging from 0 (representing black) to 255 (representing white) and intermediate values representing shades between black to white. With

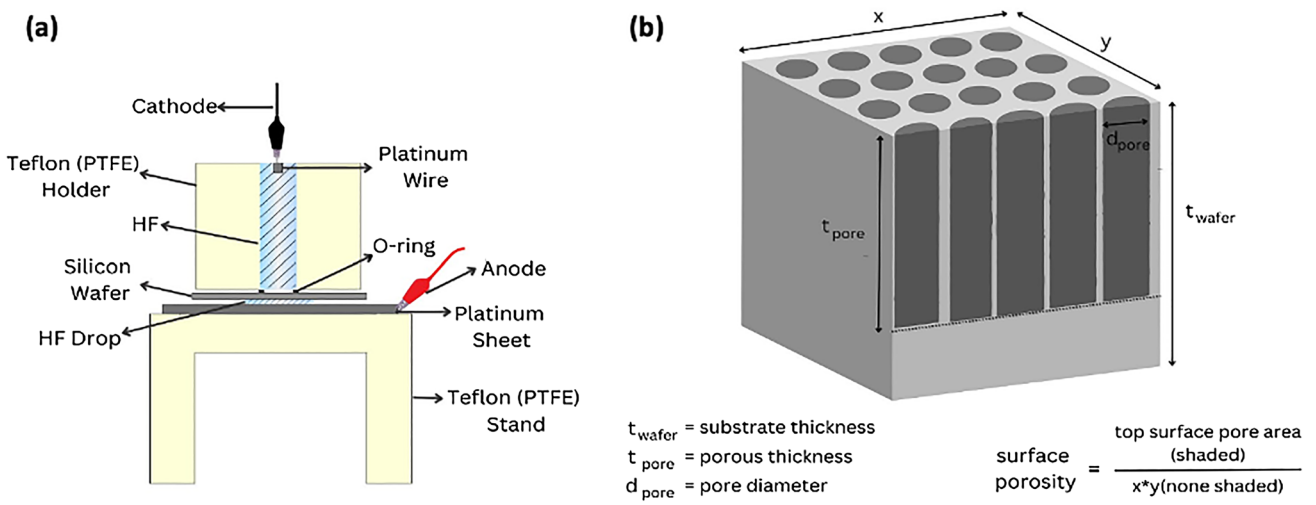

Fig. 1 **a** Single-sided cell setup for electrochemical anodization of silicon (i.e., PSi formation), **b** Porous silicon schematic illustrating the definition of surface porosity

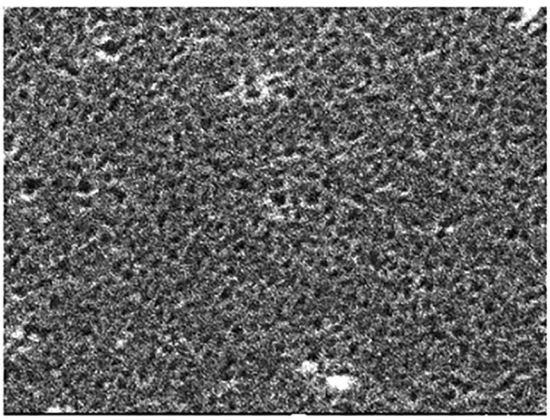

(a) Raw SEM Image

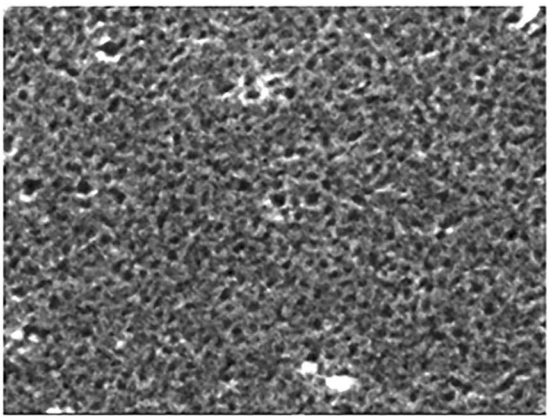

(b) Noise Reduced Image

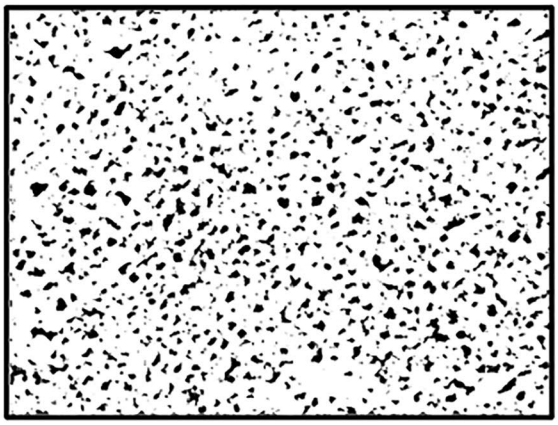

(c) Histogram Normalized ImageJ Processed Image

(d) Fabrication parameters and morphology results:

Sample ID	Current Density (mA/cm^2)	Anodization Time (s)	Porosity (%)	Target Porous Thickness (μm)	Actual Porous Thickness (μm)
Ps_1	90	672	30.2 ± 5.3	50	48.9 ± 0.7
Ps_2	90	336	26.3 ± 2.9	25	24.1 ± 0.3
Ps_3	90	134	20.5 ± 3.4	10	10.6 ± 0.2
Ps_4	90	67	19.3 ± 6.2	5	4.7 ± 0.2
Ps_5	90	13	7.7 ± 3.4	1	1.1 ± 0.1

Fig. 2 **a** Raw SEM image of one sample site used for the determination of surface porosity, **b** the noise reduced image using the median noise reduction tool in Adobe Photoshop, **c** the histogram normalized output image from ImageJ used to compute an estimate of the surface porosity by using the equation in Fig. 1b. It should be noted that the image field dimensions, hence the area, are accurately known

the shift in overall image brightness, the histogram peaks were aligned, thus, giving a normalized image for which a consistent range of values represented surface pore regions (i.e., darker regions). See Fig. 2c. This selected range was then used for all processed images to normalize the pixel selection process from sample to sample. Finally,

the percentage of the highlighted porous area compared to the total area was derived from ImageJ, thus, yielding an estimate of the surface porosity. The surface porosity estimates from our sample set are shown in the table in Fig. 2d. Example SEM surface images from each of our five samples are shown in Fig. 3a–e. Each of the five samples required five SEM surface images for ImageJ analysis as described above.

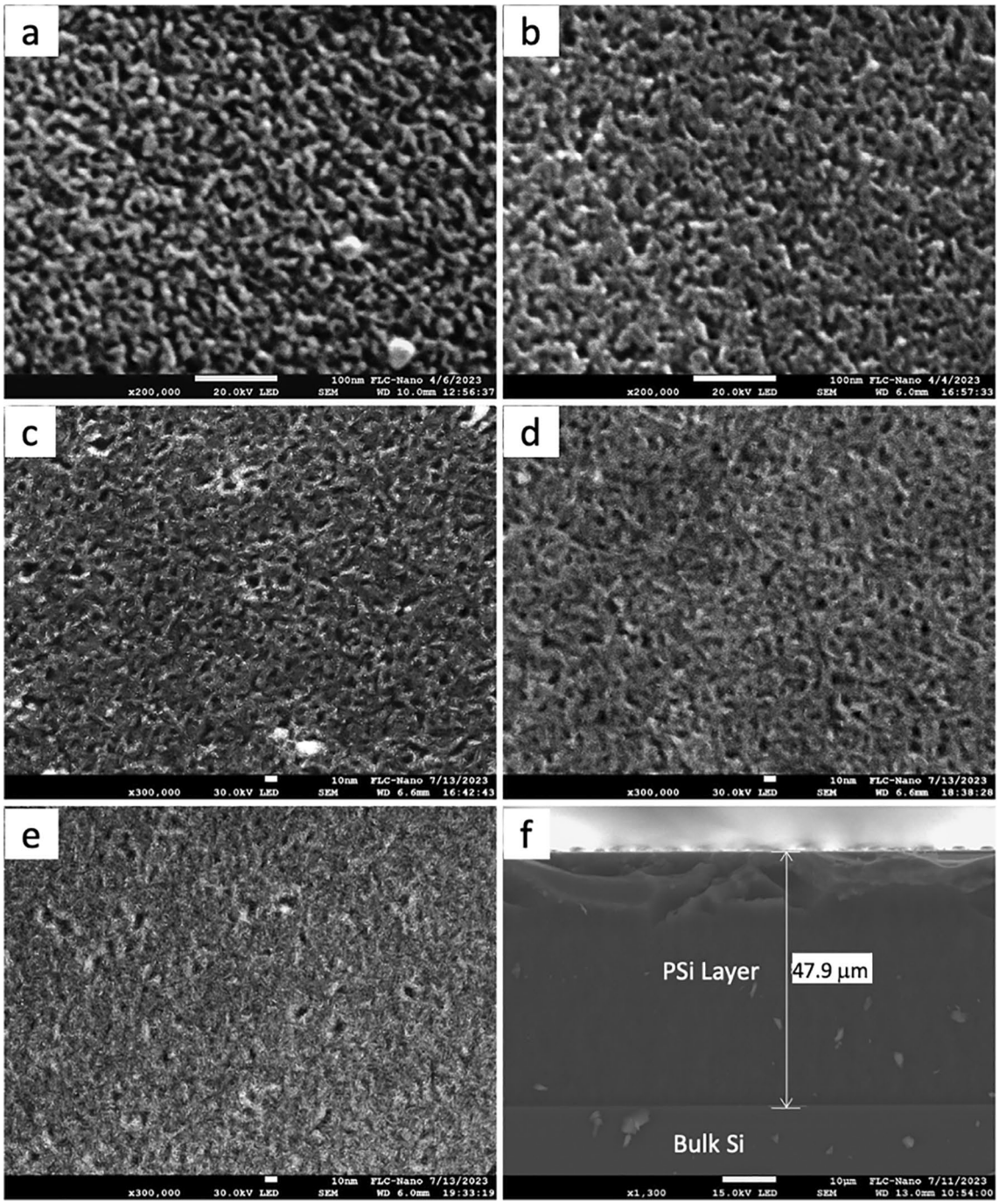

Fig. 3 The SEM images shown in **a–e** are high-magnification views of the porous silicon surfaces of one of five sites for each of the five samples produced in this study. The pore diameters range in value from approximately 4 nm to 15 nm. These samples labeled as Ps_1–Ps_5 are outlined in the table in Fig. 2d. **a** Sample Ps_1 (672 s anodization time) at 200kX magnification, **b** Sample Ps_2 (336 s anodization time) at 200kX magnification, **c** Sample Ps_3 (134 s anodization time) at 300kX magnification, **d** Sample Ps_4 (67 s anodization time) at 300kX magnification, **e** Sample Ps_5 (13 s anodization time) at 300kX magnification, **f** An example SEM image showing the cross section of the porous silicon on bulk silicon produced in this study. This image is from sample Ps_1

Characterization of the mechanical properties

To determine the mechanical properties of the porous silicon for comparison to biological membranes, nanoindentation experiments were conducted using a Hysitron TI-950 Triboindenter. The indenter utilized a Berkovich geometry probe with an included angle of 142.3° and a radius of curvature of approximately 150 nm. Prior to the experiments, the tip area function was calibrated using a fused quartz reference. Indents were performed using a trapezoidal waveform input (5 s load to 100 nm maximum depth, hold for 2 s, and 5 s unload). For our indentation experiments, a peak depth of 100 nm was selected to not exceed 1/10th of the film thickness to minimize the influence of the substrate on which the membrane was affixed during the nanomechanical measurements [8–10].

Five distinct samples were evaluated, all obtained from the same batch of silicon wafers and subjected to the same cleaning procedure. As described above, the fabrication process involved the use of a single-sided anodization cell.

The indenter was carefully positioned at the edge of the center point for each sample. Nanoindentation was then conducted at three distinct sites on every sample. The nanoindentation process followed a systematic sequence of indentations at specific distances. Initially, a set of five indentations were performed at the center of the sample. Subsequently, another set of five indentations was carried out at a distance of 700 nm to the right from the center point, followed by a final set of five indentations at 700 nm to the left from the center point. In total, 15 nano-indentations were performed per sample at three different sites. The reduced modulus (E_r) of the material at each indentation site was determined by an Oliver and Pharr analysis of the unloading curve [11].

$$E_r = \left(\frac{\left(1 - \nu_{sample}^2\right)}{E_{sample}} + \frac{\left(1 - \nu_{indenter}^2\right)}{E_{indenter}} \right)^{-1},$$

where E_{sample} is the modulus of the sample, $E_{indenter}$ is the modulus of the indenter, ν_{sample} is the Poisson's ratio of the sample, and ν_{indenter} is the Poisson's ratio of the indenter.

Results and discussion

The nanoindentation instrument used for mechanical studies requires the sample to be securely fastened to the sample stage. Due to this, we chose to partially etch our samples, creating the porous silicon layer sitting on top of a bulk silicon substrate to measure the mechanical properties of the porous silicon in our membranes. Varying anodization times were applied to generate samples (designated as Ps_1 – Ps_5) with different pore depths. A representative SEM cross-sectional image used to measure pore depth is shown in Fig. 3f. Specifically, the targeted pore depths for the samples were set at 50 µm, 25 µm, 10 µm, 5 µm, and 1 µm. The actual measured depths and corresponding anodization times are reported in Fig. 2d. The range of PSi thicknesses was chosen for a number of reasons. First, our previously reported studies targeted thinned membranes in the 25 µm to 50 µm range so we generated similar thicknesses for comparison. Second, the interstitial space in the human lung that the membrane is to mimic is on the order of 1 µm thick. And lastly, thicknesses of at least 1 µm were used to allow for an indentation depth of 100 nm not to exceed the 1/10th limit before substrate effects were detected.

The experimental results regarding the morphology of the samples are presented in the table of Fig. 2d. These results are comparable to previous studies on porous silicon that utilized similar anodization methods. In a previous study by Fakiri et al. [10], various current densities ranging from 20 to 80 mA/cm^2 were utilized, along with anodization times varying from 5400 to 1800 s. As a result, this study observed porosity levels in the range of 38% to 68% with a general decrease in Young's modulus and hardness as porosity was increased. Comparatively, in our research, we employed a current density of 90 mA/cm^2 and shorter anodization times. Our obtained porosity values ranging from 7.7% to 30.1% aligned with these prior findings thus demonstrating comparability with other studies.

The nanoindentation results of each sample were correlated with their respective experimentally estimated surface porosity. The findings revealed an inverse proportionality between the reduced modulus (E_r) and surface porosity as shown in Fig. 4a. $\boldsymbol{E_r}$ would, therefore, decrease as the porosity increases (*i.e.,* more void space in the volume) which is consistent with other reported studies [9, 10]. Figure 4b depicts the relationship between estimated surface porosity and pore depth of the analyzed samples. The observed trend appears to suggest that an increase in pore depth corresponds to an increase in surface porosity. This is also observed by careful inspection of the images such as the ones shown in Fig. 3(***a*** **–** ***e***). However, we expect that the pore depth and surface porosity should be independent of each other. The perceived correlation may be attributed to longer anodization causing a rougher surface, and roughness can be mistaken for pores using the image processing technique employed in this study.

Fakiri et al. [10] reported the modulus of their porous silicon film on a bulk silicon substrate to be in the range of 20 GPa to 57 GPa. Their research shares similarities with our own in terms of fabrication techniques and methodologies. In our experiment, the modulus of the porous silicon film on a bulk silicon substrate was lower, ranging from 6.8 to

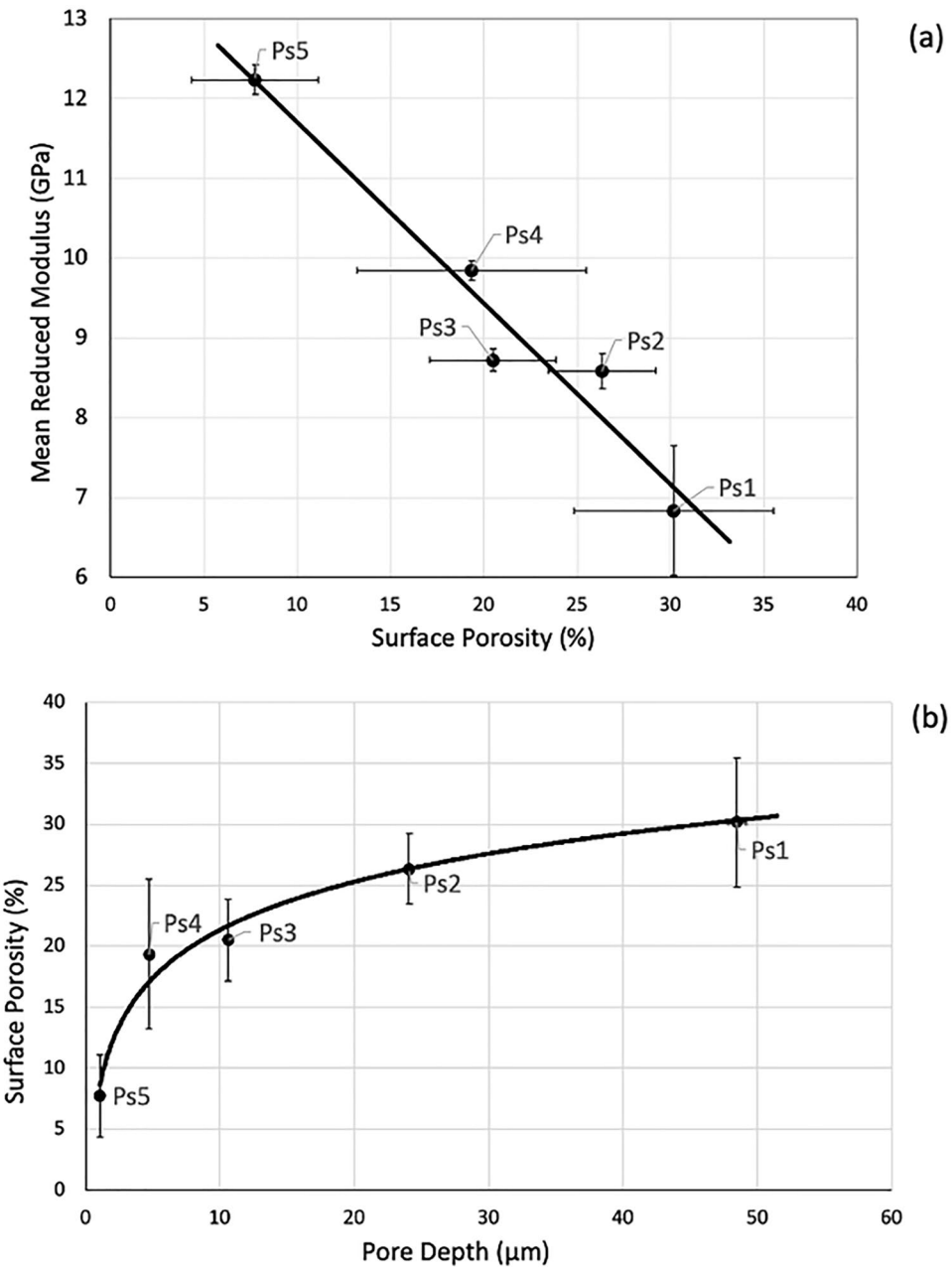

Fig. 4 **a** Mean-reduced modulus versus estimated surface porosity. **b** Estimated surface porosity on each sample versus the measured pore depth. For all cases, the error bars represent the standard deviation. It should be noted that at the scale of the plots, some of the error bars are not obvious (e.g., for pore depth)

12.2 GPa, but within the same order of magnitude. Further, it should be noted that compared to our results, other studies that investigated artificial membranes, such as PDMS porous bio membranes investigated by Huh et al. [3, 5] and others [12, 13] have reported lower moduli within the MPa range. Other groups have reported human lung tissue interstitial space elastic moduli in the KPa range [14–16].

We recognize the need for further investigations and data collection in our future work. Future work will focus on determining the properties (mechanical, chemical, and biological) of free-standing, thin porous silicon membranes (less than 5 µm) that will more closely match the anatomical thickness of a human interstitial space (~ 1 µm), thusly, allowing a better comparison of properties between our engineered membrane and biological membranes. In addition, we intend to explore the relationship between pore depth and surface porosity by imaging and calculating the cross-section porosity to provide valuable insights into the expected independence of these parameters.

This study presents ongoing work towards the fabrication of a reproducible porous silicon bio membrane that mimics the interstitial space in the lungs. The mechanical and morphological characterization of the membrane using scanning electron microscopy and nanoindentation provides important insights for optimizing the fabrication process and developing Lung-on-a-Chip models for personalized medicine.

Supplementary Information The online version contains supplementary material available at https://doi.org/10.1557/s43580-023-00667-2.

Acknowledgments We would like to thank the faculty in the Fort Lewis College Department of Physics & Engineering specifically, Jerry Crawford and Yiyan Li for their generosity and expertise throughout this project. The success of this work was made possible with guidance and expertise provided by Fort Lewis College shop manager Jason Wagner and Lab Coordinator Carl Bickford. We would also like to thank Marcus A. C. Williams, Cooper Wiens, Adam Hamilton, Sophie Mancha, Madeline Stalder, Koby Vargas, Sofia Maines, Julia Earley, and Aaron Simien for their past contributions. This work would not have been possible without the support of grant coordinator Jaimee McCullough. This project was graciously funded by the NSF PREM for Functional Nanomaterials [Award #1827847], STROBE NSF Science and Technology Center for Real-Time Functional Imaging [Award #1548924] and NIH BLaST Biomedical Learning and Student Training [Award # RL5GM118990]. Nanoindentation was performed at the MIMIC Facility, University of Colorado, Boulder (RRID:SCR_019307).

Author contributions SG: Formal Analysis, Methodology, Validation, Investigation, Data Curation, Visualization, Resources, Software, Writing—Original Draft. ST: Investigation, Methodology, Validation, Visualization, Writing—Review & Editing. OH: Investigation, Methodology, Validation, Software, Visualization, Writing—Review & Editing. LG: Formal Analysis, Data Curation, Investigation, Methodology, Validation, Software, Visualization, Writing—Review & Editing. DR: Formal Analysis, Data Curation, Investigation, Methodology, Validation, Software, Visualization. FS: Investigation, Methodology, Validation, Visualization, Writing—Review & Editing. AM: Formal Analysis, Investigation, Methodology, Validation, Visualization, Writing—Review & Editing. SMS: Formal Analysis, Methodology, Validation, Supervision, Visualization, Writing-Original Draft. AG: Formal Analysis, Investigation, Validation, Software, Writing—Review & Editing, Supervision. VLF: Formal Analysis, Validation, Resources, Writing—Review & Editing, Supervision. JJ: Formal Analysis, Methodology, Conceptualization, Validation, Investigation, Writing—Original Draft, Visualization, Supervision, Project Administration, Resources, Funding Acquisition.

Funding This project was graciously funded by the NSF PREM for Functional Nanomaterials [Award #1827847] supporting Sahra Genc, Sally Thompson, Owen Hill, Leif Gislason, Dakota Rodriguez, Farjana Showme, Alex Motler, Sarah M. Schreiner, and Jeff Jessing; STROBE NSF Science and Technology Center for Real-Time Functional Imaging [Award #1548924] supporting Sahra Genc, Sally Thompson, Owen Hill, Leif Gislason, Dakota Rodriguez, Farjana Showme, Alex Motler, Sarah M. Schreiner, and Jeff Jessing; and NIH BLaST Biomedical Learning and Student Training [Award # RL5GM118990] supporting Sahra Genc and Jeff Jessing. Nanoindentation was performed at the MIMIC Facility, University of Colorado, Boulder (RRID:SCR_019307).

Data availability The datasets generated during and analyzed during the current study are available from the corresponding author on reasonable request.

Declarations

Conflict of interest The authors declare that they have no known competing financial interests or personal relationships that could have appeared to influence the work reported in this paper.

References

1. Y. Buhidma, K. Rukavina, K.R. Chaudhuri, S. Duty, Potential of animal models for advancing the understanding and treatment of pain in Parkinson's disease. NPJ Parkinson's Dis. (2020). https://doi.org/10.1038/s41531-019-0104-6
2. A. Pearce, R. Richards, S. Milz, E. Schneider, S. Pearce, Animal models for implant biomaterial research in bone: A review. Eur. Cells Mater. **13**, 1–10 (2007). https://doi.org/10.22203/ecm.v013a01
3. D. Huh, H.J. Kim, J.P. Fraser, D.E. Shea, M. Khan, A. Bahinski, G.A. Hamilton, D.E. Ingber, Microfabrication of human organs-on-chips. Nat. Protoc. **8**(11), 2135–2157 (2013). https://doi.org/10.1038/nprot.2013.137
4. D.E. Ingber, Reverse engineering human pathophysiology with organs-on-chips. Cell **164**(6), 1105–1109 (2016). https://doi.org/10.1016/j.cell.2016.02.049
5. D. Huh, B.D. Matthews, A. Mammoto, M. Montoya-Zavala, H.Y. Hsin, D.E. Ingber, Reconstituting organ-level lung functions on a chip. Science **328**(5986), 1662–1668 (2010). https://doi.org/10.1126/science.1188302
6. M. Williams, C. Wiens, A. Hamilton, S. Mancha, M. Stalder, K. Vargas, J. Crawford, Y. Li, S.M. Schreiner, D. Blake, J.R. Jessing, Novel fabrication approach of a porous silicon biocompatible membrane evaluated within a alveolar coculture model, 2021. https://doi.org/10.31224/osf.io/mztyc.
7. W.S. Rasband, ImageJ, U. S. National Institutes of Health, Bethesda, Maryland, USA, 1997–2018. https://imagej.nih.gov/ij/.
8. H. Bückle, Progress in micro-indentation hardness testing. Metall. Rev. **4**(1), 49–100 (1959). https://doi.org/10.1179/095066059790421746
9. A. Zocco, A. Perrone, E. Broitman, Z. Czigany, L. Hultman, M. Anderle, N. Laidani, Mechanical and tribological properties of CNx films deposited by reactive pulsed laser ablation. Diam. Relat. Mater. **11**(1), 98–104 (2002). https://doi.org/10.1016/s0925-9635(01)00527-1
10. S. Fakiri, A. Montagne, K. Rahmoun, A. Iost, K. Ziouche, Mechanical properties of porous silicon and oxidized porous silicon by nanoindentation technique. Mater. Sci. Eng. A **711**, 470–475 (2018). https://doi.org/10.1016/j.msea.2017.11.013
11. D.J. Shuman, A.L.M. Costa, M.S. Andrade, Calculating the elastic modulus from nanoindentation and microindentation reload curves. Mater Charact **58**(4), 380–389 (2007). https://doi.org/10.1016/j.matchar.2006.06.005
12. J. Wala, D. Maji, S. Das, Influence of physico-mechanical properties of elastomeric material for different cell growth. Biomed. Mater. **12**(6), 065002 (2017). https://doi.org/10.1088/1748-605x/aa7e81
13. J.H. Wen, L.G. Vincent, A. Fuhrmann, Y.S. Choi, K.C. Hribar, H. Taylor-Weiner, S. Chen, A.J. Engler, Interplay of matrix stiffness

and protein tethering in stem cell differentiation. Nat. Mater. **13**(10), 979–987 (2014). https://doi.org/10.1038/nmat4051
14. A.J. Booth, R. Hardley, A.M. Cornett, A.A. Dreffs, S.A. Matthes, J.L. Tsui, K. Weiss, J.C. Horowitz, V.F. Fiore, T.H. Barker, B.B. Moore, F.J. Martinez, L.E. Niklason, E.S. White, Acellular normal and fibrotic human lung matrices as a culture system for in vitro investigation. Am. J. Respir. Crit. Care Med. **186**(9), 866–876 (2012). https://doi.org/10.1164/rccm.201204-0754oc
15. D. Sicard, A.J. Haak, K.M. Choi, A.R. Craig, L.E. Fredenburgh, D.J. Tschumperlin, Aging and anatomical variations in lung tissue stiffness. Am. J. Physiol. **314**(6), L946–L955 (2018). https://doi.org/10.1152/ajplung.00415.2017
16. S.R. Polio, A.N. Kundu, C.E. Dougan, N.P. Birch, D.E. Aurian-Blajeni, J.D. Schiffman, A.J. Crosby, S.R. Peyton, E. Dague, Cross-platform mechanical characterization of lung tissue. PLoS ONE **13**(10), e0204765 (2018). https://doi.org/10.1371/journal.pone.0204765